

Robust Multispectral Palmprint Identification System by Jointly Using Contourlet Decomposition & Gabor Filter Response

Abdallah Meraoumia¹, Salim Chitroub² and Ahmed Bouridane³

¹Univ Ouargla, Fac. des nouvelles technologies de l'information et de la communication,
Lab. de Génie Électrique, Ouargla 30 000, Algeria

²Signal and Image Processing Laboratory, Electronics and Computer Science Faculty, USTHB,
P.O. box 32, El Alia, Bab Ezzouar, 16111, Algiers, Algeria

³Department of Computer Science and Digital Technologies, Northumbria University Newcastle,
Pandon Building, Newcastle upon Tyne NE2 1XE, U.K.

Keywords: Biometrics, Identification, Multispectral Palmprint, Contourlet, HMM, Gabor Filter, Data Fusion.

Abstract: In current society, reliable identification and verification of individuals are becoming more and more necessary tasks for many fields, not only in police environment, but also in civilian applications, such as access control or financial transactions. Biometric systems are used nowadays in these fields, offering greater convenience and several advantages over traditional security methods based on something that you know (*password*) or something that you have (*keys*). In this paper, we propose an efficient online personal identification system based on Multi-Spectral Palmprint (MSP) images using Contourlet Transform (CT) and Gabor Filter (GF) response. In this study, the spectrum image is characterized by the contourlet coefficients sub-bands. Then, we use the Hidden Markov Model (HMM) for modeling the observation vector. In addition, the same spectrum is filtered by the Gabor filter. The real and imaginary responses of the filtering image are used to create another observation vector. Subsequently, the two sub-systems are integrated in order to construct an efficient multi-modal identification system based on matching score level fusion. Our experimental results show the effectiveness and reliability of the proposed method, which brings both high identification and accuracy rate.

1 INTRODUCTION

The automatic personal identification is becoming an increasingly important requirement in a variety of applications like access control, surveillance systems and physical buildings. In recent years, the use of biometrics has been increasingly researched as an alternative to traditional methods in the initial identification procedure. Biometrics is an emerging field of information technology that is crucial for human identification and verification. Biometric technologies measure and recognize human physical and behavioral characteristics for identification purposes (Jinrong Cui, 2011). Some of the most common physical characteristics include features extracted from hand pattern. Furthermore, the palms of the human hands contain a wide variety of features (*e.g.*, shape, texture, and principal palm lines) that can be used by biometric systems. These features of the human hand are relatively stable and the hand image from which feature are extracted can be acquired relatively easily (D. Zhang and Kumar, 2010). Therefore, in the

past few years, palmprint has attracted an increasing amount of attention. In other hand, several studies for palmprint-based personal identification systems have focused on improving the performance of palmprint images captured under visible light. However, during the past few years, some researchers have considered multispectral images to improve the effect of these systems. This technique can be give different information from the same palmprint modality using an acquisition device to capture the palmprint images under visible and infrared light resulting into several spectrum images (Cui, 2012).

In addition, several studies has demonstrated that unimodal biometric identification (that is, identification based on a single biometric characteristic) makes it difficult for an impostor to impersonate a legitimate user. More recent research is finding that multimodal biometric identification (that is, identification based on the combination of multiple algorithms) can make it even more difficult for an impostor to impersonate a legitimate user (A. Noore and Vatsa, 2007). Thus multimodal biometrics claims improved accuracy and

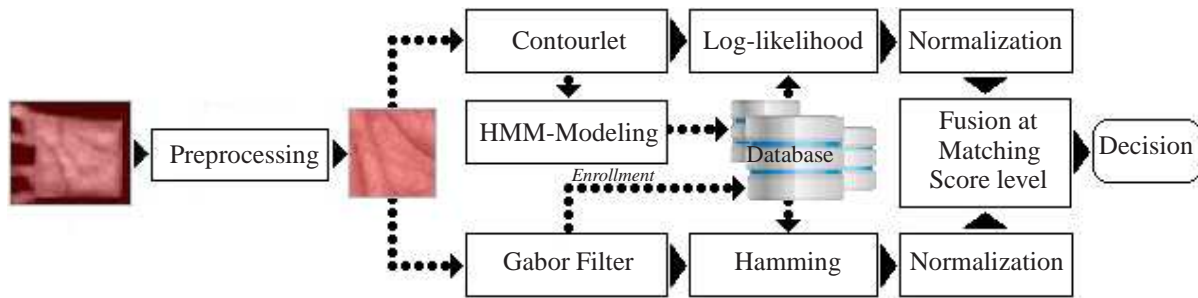


Figure 1: Multi-algorithmic palmprint identification system based on contourlet decomposition & gabor filter response.

robustness. In this paper, two palmprint identification algorithms are proposed. Thus, we first propose a multispectral palmprint identification based on single spectrum. Further, the paper presents a method for fusing information from the different spectrums and algorithms. However, multimodal biometric systems can be designed to operate in one of the following two scenarios, multiple units (Single biometric, multiple units) and multiple algorithms (Single biometric, multiple algorithms). The rest of the paper is organized as follows. The proposed scheme of the multimodal biometric system is presented in section 2. The two proposed systems framework (contourlet based identification system and Gabor filter response based identification system) are given in section 3. The normalization and fusion process used for fusing the information is detailed in section 4. In section 5, the experimental results, prior to fusion and after fusion, are given and commented. Finally, the conclusions and further works are presented in sections 6.

2 PROPOSED IDENTIFICATION SYSTEM

Fig. 1 illustrates the various modules of the proposed multimodal biometric identification system based on *RED* spectrum (multi-algorithmic based multimodal biometric identification system). The proposed system is composed of two different unimodal sub-systems exchanging information in matching score level. Each sub-system exploits different algorithms (*CT* and *GF*). The proposed multi-algorithmic based multimodal identification system consists of pre-processing process, matching process (log-likelihood scores given each model for the first sub-system and Hamming distance in the case of second sub-system), normalization and decision process.

To enroll into the first sub-system database, the user has to provide a set of training spectrums. Typically, an observation vector is extracted from each

spectrum which describes certain characteristics using *CT* technique and modeling using *HMM*. Finally, the models parameters are stored as references models. For identification, the same observation vectors are extracted from the test spectrum images and the log-likelihood is computed using all of models references in the database.

In the case of the second sub-system, a feature vector is extracted from each spectrum image by using the 2D Gabor filter response and encoding step. Then, the extracted feature vectors are stored as reference templates. For identification phase, the same feature vectors are extracted from the test spectrum images, then, the Hamming distance (matching module,) is computed using all of reference templates in the system database. For both sub-systems, and based on the resulting fusion of the obtained normalized matching scores, a decision of accepting or rejecting the user is then made.

3 SYSTEMS FRAMEWORK

After the image is captured, it is pre-processed to obtain only the area information of each spectrum. In the palmprint preprocessing, a Region Of Interest (*ROI*) has to be located from the original spectrum image before further feature extraction, using the method described in (David Zhang and Zuo, 2010). In our method, the features are generated by the *CT* and *GF* techniques.

3.1 Contourlet Based Identification System

The spectrum image is typically analyzed using the *CT* method. Thus, to create an observation vector, the spectrum image is transformed into a sub-bands form (using *CT* into one level). Fig. 2 shows the feature vector extraction methods using a contourlet decomposition with one levels. The palmprint feature vectors (each spectrum) are created by combining

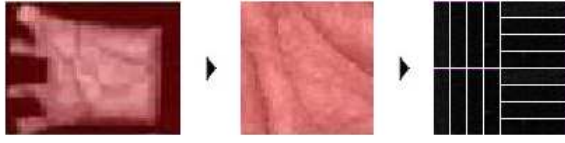


Figure 2: Observation vector generation using one level contourlet decomposition. (left) RED spectrum image, (middle) Input of ROI sub-image and (right) Feature vector extraction.

some bands extracted using contourlet decomposition (Singh and Mishra, 2011). After that, this vector is compressed using Principal Components Analysis (PCA) method and some of principal components are selected for representing the final observation vectors. Finally, an HMM model of each observation vector is constructed. Note that, in order to find the best parameters of the ergodic HMM model (Harun Uguz, 2007), we choose empirically the number of gaussian in the Gaussian Mixture Model (GMM) equal to 1 and the number of states of the HMM equal to 6.

In the matching process, after extracting the observation vectors corresponding to the test spectrum image, the probability of the observation sequence given a HMM model is computed via a viterbi recognizer. The model with the highest log-likelihood is selected and this model reveals the identity of the unknown palmprint (person). Thus, during the identification process, the characteristics of the test spectrum image are extraction. Then the log-likelihood score of the observation vectors, O_i , given each model, λ_j , is computed. Therefore, the resulting score is given by:

$$d_{ij}^L = P(O_i|\lambda_j) = \ell(O_i, \lambda_j) \quad (1)$$

where $j = 1 \dots N$ and N represents the size of model database.

3.2 Gabor Based Identification System

In this system, the features are generated from the ROI sub-images by filtering the spectrum image with 2D Gabor filter (Angel Serrano, 2010). This feature extraction technique has been widely used for pattern recognition. Thus, the response of a Gabor filter to an image is obtained by a 2D convolution operation. Fig. 3 shows the feature vector extraction methods using a Gabor filter response at an orientation $\theta = \frac{\pi}{4}$. The $M \times M$ Gabor filter, $M = 16$, at an orientation, $\theta = \frac{\pi}{4}$, will convolute with the ROI sub-images. The results of a pair of a real and an imaginary filter are combined in the Gabor phase response ϕ as follows:

$$\phi_{\theta, \mu, \sigma} = \tan^{-1} \left(\frac{\text{Im}(S_{\theta, \mu, \sigma})}{\text{Re}(S_{\theta, \mu, \sigma})} \right) \quad (2)$$

The Gabor phase response is qualitatively encoded as “0” or “1” based on the sign. therefore, the

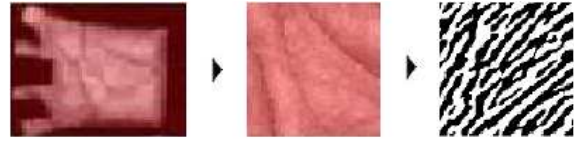


Figure 3: Observation vector generation using Gabor filter response. (left) RED spectrum image, (middle) Input of ROI sub-image and (right) Binary observation vector.

binary template, $\psi(i, j)$, is represented by the following inequalities :

$$\psi(i, j) = \begin{cases} 0 & \text{if } \phi_{\theta, \mu, \sigma}(i, j) < 0 \\ 1 & \text{if } \phi_{\theta, \mu, \sigma}(i, j) \geq 0 \end{cases} \quad (3)$$

Note that, in the experiments, M , μ and σ are set as 16, 0.0916 and 5.6179, respectively, are used in all calculation.

The criterion for similarity/dissimilarity is to minimize the distance between the input binary template ψ_i and the stored binary templates ψ_j . The difference between the templates is labeled “Hamming Distance” (Xian-Qian Wu, 2003). A simple XOR operation between the corresponding pair of templates provides this Hamming distance. Hamming distance does not measure the difference between the components of the feature vectors, but the number of components that differ in value. We can define the hamming distance, d^H , by the following formula:

$$d_{ij}^H = \frac{1}{H_s \cdot W_s} \sum_{n=1}^{n=H_s} \sum_{m=1}^{m=W_s} \psi_i(n, m) \oplus \psi_j(n, m) \quad (4)$$

where $j = 1 \dots N$ and N represents the size of template database. The \oplus is the exclusive OR operator (XOR) and $H_s \times W_s$ is the size of the templates. The value d_{ij}^H lies between 0 and 1, inclusive, with 1 meaning that the two templates are independent and 0 meaning they are identical.

4 NORMALIZATION & FUSION PROCESS

4.1 Normalization Process

During the identification process, two sub-systems are used, a fusion sub-system will have to take into consideration the fact that the scores to be combined are of different types, e.g., a CT based sub-system which outputs scores in the range $[0, 10^4]$, a GF based sub-system which outputs scores in the range $[0, 1]$. In this respect, the system outputs are mapped into a common score representation (score normalization) before they are combined. Thus, the matching score,

d , between the test spectrum image, and all of reference templates (models) in the system database are computed, therefore the vector scores, \mathcal{V} , given all these distance is given as:

$$\mathcal{V} = [d_1 \ d_2 \ d_3 \ d_4 \cdots d_N] \quad (5)$$

where $d_j = d_j^L$ or d_j^H . An important aspect that has to be addressed in identification process is the normalization of the scores obtained. Thus, a *Min-Max* normalization scheme was employed to transform the scores computed into similarity scores in the same range (Jinrong Cui, 2011).

$$\tilde{\mathcal{V}} = \frac{\mathcal{V} - \min(\mathcal{V})}{\max(\mathcal{V}) - \min(\mathcal{V})} \quad (6)$$

where $\tilde{\mathcal{V}}$ denotes the normalized scores. However, these scores are compared, and the lowest/highest score is selected. Therefore, the best score is D_o and its equal to:

$$D_o = \begin{cases} \max(\tilde{\mathcal{V}}) & \text{for the first sub-system} \\ \min(\tilde{\mathcal{V}}) & \text{for the second sub-system} \end{cases} \quad (7)$$

Finally, this score is used for decision making. Not that, for fusing the two sub-systems, it must converting the log-likelihood scores, d_j^L , to another scores (similar to the Hamming distance) by,

$$\hat{d}_{ij}^L = 1 - d_{ij}^L \quad (8)$$

4.2 Fusion Process

There are several methods to combine multimodal information. These methods are known as fusion techniques. Fusing information at the score level is interesting because it reduces the problem complexity by allowing different sub-systems to be used independently of each other. However, in the multimodal system design, these modalities operate independently and their results are combined using an appropriate fusion scheme. Thus, the fusion of the two sub-systems is realized using five simple rules (Anil Jain, 2005). These rules consist of the sum (*SUM*) and weighted-sum (*WHT*) of the two similarity measures, their minimum (*MIN*) and maximum (*MAX*) of both and finally their multiplication (*MUL*). The final decision of the multimodal system is then given by choosing the person, which minimizes the fused similarity measures between the sample and the matching base.

5 EXPERIMENTAL RESULTS AND DISCUSSION

5.1 Experimental Database

The proposed methods are validated on multispectral palmprint database from the Hong Kong polytechnic university (PolyU) (PolyU,). The database contains images captured with visible and infrared light. Four spectrum images for each person, including *Red*, *Green*, *Blue* and *near-infrared* spectrum (Fig. 4), are collected. 6000 multispectral palmprint images were collected from 500 persons. These images were collected in two separate sessions. In each session, the person provide 6 images for each palm, so there are 12 images for each person. Therefore, 48 spectrum images of all illumination from 2 palms were collected from each person. The average time interval between the first and the second sessions was about 9 days.



Figure 4: Samples of multispectral palmprint.

5.2 Simulation Results

In the system-design phase (all experiments), three images are randomly selected of twelve images of each class (person) were used in the enrolment stage to create the system database. In the following tests, we setup a database with size of 400 classes, which are similar to the number of employees in small to medium sized companies. Thus, the client experiments were performed by comparing nine test images with the corresponding class in the database. A total of 3600 comparisons were made. The impostor experiments were performed by comparing the nine images with each class in the database. A total of 718200 impostor experiments were made

5.2.1 Unimodal Identification Systems

GF Based Identification System The goal of this experiment was to evaluate the system performance when we using information from each spectrum with *GF* algorithm. For the *open set* identification, we found the performance under different spectrums (*Red*, *Green*, *Blue*, *Near-infrared*). By adjusting the matching threshold, a Receiver Operating Characteristic (*ROC*) curve, which is a plot of False Reject Rate

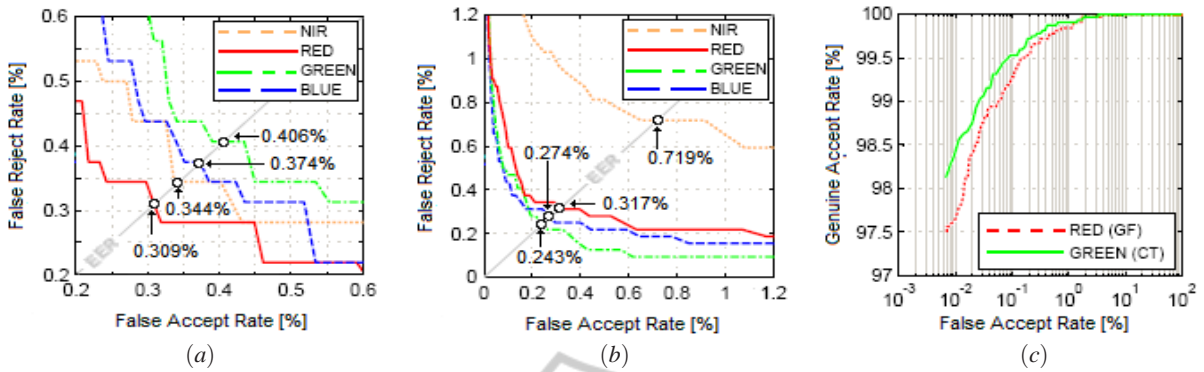


Figure 5: Unimodal identification system performance. (a) The ROC curves with respect to the different spectrums, using Gabor filter response, (b) The ROC curves with respect to the different spectrums, using contourlet decomposition and (c) Comparison between the best systems.

Table 1: Unimodal Identification Systems Test Results.

RULE	OPEN SET IDENTIFICATION PERFORMANCES				CLOSED SET IDENTIFICATION PERFORMANCES			
	GF		CT		GF		CT	
	T_o	EER	T_o	EER	ROR	RPR	ROR	RPR
RED	0.2583	0.309	0.9154	0.317	98.000	107	97.656	341
GREEN	0.2642	0.406	0.9173	0.243	96.500	118	98.219	240
BLUE	0.2490	0.374	0.9173	0.274	96.469	94	98.063	78
NIR	0.2896	0.344	0.8905	0.719	97.438	137	96.813	271

(FRR) against False Accept Rate (FAR) for all possible thresholds, can be created. Fig. 5.(a) compares the performance of the system for varying spectrum types. From Fig. 5.(a) it can be seen that the Red spectrum perform better than the other spectrums in terms of Equal Error Rate (EER). Thus, the GF based unimodal open set identification system can be work with a minimum error, EER, equal to 0.3091% at a threshold $T_o = 0.2583$. Finally, Table 1 (first line) illustrates the experimental results for all spectrum images.

For the evaluation of the closed set identification system performance, Table 1 (first line) presents the average identification results for all spectrums. From this Table, it can be seen that always the Red spectrum offers the best identification rate with a Rank-One Recognition (ROR) equal to 98.000 % and a Rank of Perfect Recognition (RPR) of 107.

CT Based Identification System In this section, we performed a simulation using the experimental settings as before but this time, we varied the feature extraction technique (by using CT). Therefore, as mentioned above, the observation vector is composed of PCA features extracted from the transformed spectrum image columns. Thus, as know, the principal component vectors reflect the compact information of different column vectors. Most of these vectors they become negligible, as result; the vector derived from

the initial vectors computation is limited to an array of summed vectors within all components. The test was repeated for various numbers of components, only 64 component (99.956 % of the total information) are enough to achieve good identification rate. So, we conducted several experiments to investigate the effectiveness of the spectrum types (choose the spectrum type yield the best performance). For this, we found the performance under different spectrums and the results are illustrated in Fig. 5.(b). The obtained experimental results show that this open set identification sub-system works best using Green spectrum with an EER equal to 0.2430 % at $T_o = 0.9173$. The results for all spectrum images are shown in Table 1.

The closed set identification sub-system are shown in Table 1. As can be observed, Green spectrum give the best identification rate (ROR = 98.2188 and RPR = 240). Finally, to find the better open set identification systems, graphs showing the ROC curves for the open set identification using GF and CT based unimodal systems, were generated (see Fig. 5.(c)). By the analysis of this plot, it can be observed that the performance of the unimodal open set identification system is significantly improved by using the CT method.

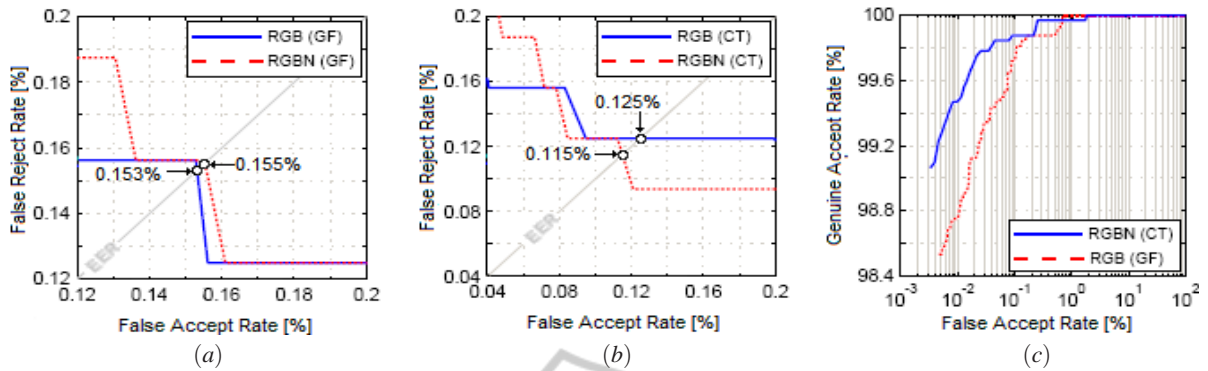


Figure 6: Multiple-units based multimodal identification system performance. (a) The ROC curves with respect to the two combinations (RGB and RGBN), using Gabor filter response, (b) The ROC curves with respect to the two combinations (RGB and RGBN), using contourlet decomposition and (c) Comparison between the best systems.

Table 2: Mult-units Based Multimodal Identification Systems Test Results (Open Set Identification).

RULE	RGB				RGBN			
	GF		CT		GF		CT	
	T_0	EER	T_0	EER	T_0	EER	T_0	EER
SUM	0.2583	0.153	0.9151	0.125	0.2521	0.155	0.8990	0.115
WHT	0.2573	0.156	0.9164	0.125	0.2503	0.156	0.9060	0.125
MUL	0.0180	0.156	0.7942	0.125	0.0042	0.162	0.7087	0.125
MAX	0.3224	0.189	0.9455	0.125	0.3367	0.219	0.9483	0.125
MIN	0.1988	0.250	0.8981	0.168	0.1950	0.281	0.8727	0.219

Table 3: Mult-units Based Multimodal Identification Systems Test Results (Closed Set Identification).

RULE	RGB				RGBN			
	GF		CT		GF		CT	
	ROR	RPR	ROR	RPR	ROR	RPR	ROR	RPR
SUM	98.500	35	98.875	341	98.500	45	99.031	192
WHT	98.438	35	98.688	341	98.500	45	98.625	341
MUL	97.125	37	98.656	341	96.844	43	98.656	341
MAX	98.281	89	98.188	130	98.438	83	97.531	145
MIN	97.125	85	98.656	341	96.844	68	98.656	191

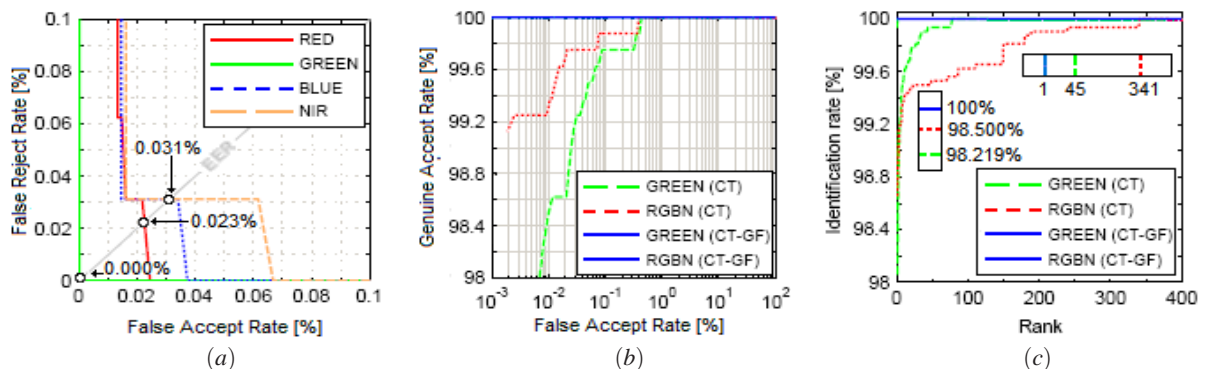


Figure 7: Multiple-algorithms based multimodal identification system performance. (a) The ROC curves with respect to the different spectrums, (b) The ROC curves, which is a plot of GAR against FAR, for all best systems and (c) The CMC curves for all best systems.

Table 4: Mult-algorithms Based Multimodal Identification Systems Test Results (Open Set Identification).

RULE	RED		GREEN		BLUE		NIR	
	T_o	EER	T_o	EER	T_o	EER	T_o	EER
SUM	0.6930	0.344	0.8863	0.014	0.8262	0.044	0.7205	0.188
WHT	0.6919	0.344	0.9930	0.000	0.8300	0.031	0.7164	0.188
MUL	0.5332	0.344	0.7677	0.029	0.7076	0.059	0.5771	0.188
MAX	0.9832	0.023	0.9751	0.031	0.9749	0.031	0.9789	0.031
MIN	0.7876	0.079	0.7989	0.103	0.8115	0.094	0.8011	0.095

Table 5: Mult-algorithms Based Multimodal Identification Systems Test Results (Close Set Identification).

RULE	RED		GREEN		BLUE		NIR	
	ROR	RPR	ROR	RPR	ROR	RPR	ROR	RPR
SUM	99.250	341	99.625	8	99.625	240	98.969	180
WHT	99.250	341	99.938	2	99.906	240	99.563	180
MUL	99.250	341	99.594	3	99.594	240	99.500	180
MAX	98.156	5	97.375	4	97.531	6	98.125	6
MIN	99.469	9	99.156	81	99.438	3	99.313	68

Table 6: Multimodal Identification Systems Using Jointly Multi-units and Multi-algorithms Methods.

RULE	OPEN SET IDENTIFICATION PERFORMANCES				CLOSED SET IDENTIFICATION PERFORMANCES			
	RGB		RGBN		RGB		RGBN	
	T_o	EER	T_o	EER	ROR	RPR	ROR	RPR
SUM	0.000	0.9796	0.000	0.9607	100.00	1	100.00	1
WHT	0.000	0.9960	0.000	0.9990	99.938	2	100.00	1
MUL	0.000	0.9558	0.000	0.8000	100.00	1	100.00	1
MAX	0.027	0.9990	0.042	0.9990	96.688	4	95.781	4
MIN	0.000	0.9614	0.000	0.9245	100.00	1	100.00	1

5.2.2 Multimodal Identification Systems

These experiments can be divided into three categories: (i) multiple-units (Single biometric, multiple units), (ii) multiple-algorithms (Single biometric, multiple algorithms) and (iii) multiple-units-algorithms (Single biometric, multiple units and multiple algorithms).

In order to see the performance of the *open/closed set* multimodal identification system, case of (i) multiple-units, we present, in table 2 and 3, the results for all combinations (RGB and RGBN) and fusion rules for the two feature extraction methods (GF and CT). These two tables shows that the SUM rule with CT method and RGBN combination offers better results in terms of the EER and ROR, for the both identification modes (*open/closed set*). Fig. 6.(a) and Fig. 6.(b) compares the performance of RGB and RGBN combinations in the case of GF and CT methods, respectively. While, Fig. 6.(c) compares the two best *open set* identification systems, from this figure, it is clear that the system can works efficiency with the fusion of all spectrums (RGBN combination) with SUM rule in the case of CT method with

$EER = 0.1151\%$ at $T_o = 0.8990$. In the case of (ii) multiple-algorithms, the individual scores for GF and CT based systems are combined to generate a single scalar score, which is then used to make the final decision. Fig. 7.(a) provides the performance of the *open set* identification system for all spectrum types and fusion rules. From this figure, it is clear that our *open set* identification system achieves a best performance when using the Green spectrum and WHT fusion rule of the two sub-systems ($EER = 0.0000\%$ and $T_o = 0.9930$). These setting (Green spectrum and WHT fusion rule) always give the best performance in the *closed set* identification mode ($ROR = 99.9375\%$ and $RPR = 2$). Finally, Table 4 and 5 done all the experimental results for all spectrum types and fusion rules.

To validate our idea we have run other tests for the case of (iii) multiple-units-algorithms. Thus, to determine the best combination and fusion rule, a table contains the results can be established (see Table 6). The experiments described in table 6 suggest that generally all fusion rules, except the MAX rule, give a better *open set* identification performance (*zeroEER*) for both combinations (RGB and RGBN). For the *closed set* identification system, the best re-

sult of *ROR* is given as 100.000 % with lowest *RPR* of 1. Not that, the average increase in performance between the unimodal *open/closed set* identification system and the multimodal *open/closed set* identification system is 100 %.

5.2.3 Comparison Study

This section is dedicated to compare the performance of the best *open/closed set* identification systems described above, this can be done by showing the *ROC* curves for the *open set* identification using unimodal and multimodal systems (see Fig. 7.(b)). As can be seen by comparing these results, the accuracy of the system using *Green* spectrum and the system based on the fusion of all spectrum types (both based on the fusion of the *GF* based sub-system and *CT* based sub-system) is very much increased and can achieve *zeroEER*. Also, the Cumulative Match Curves (*CMC*) comparing all best *closed set* identification systems are plotted in Fig. 7.(c). From this figure, always, *Green* spectrum and the system based on the fusion of all spectrum types (both based on the fusion of the *GF* based sub-system and *CT* based sub-system) give the best accuracy (*ROR* = 100 %). Through an analysis of the previous results, it can be observed that in general the performance of the unimodal system is significantly improved by using the fusion of several spectrum types. In addition, experiments also demonstrate that fusion of the two algorithms performs better results.

6 CONCLUSION AND FURTHER WORK

The objective of this work is to contribute to the multimodal identification by the use of data fusion technique. Two different sub-systems derived from each spectrum were used in this study. Fusion of the two proposed unimodal sub-systems is performed at the matching score level to generate a fused matching score which is used for recognizing a palmprint image. Feature extraction process use both *GF* and *CT* methods. The experimental results, obtained on a database of 400 persons, show a very high *open/closed set* identification accuracy. They also demonstrate that combining different spectrum types or different algorithms does significantly reduce the accuracy of the system. In addition, our tests show that the multimodal system provides better *open/closed set* identification accuracy than the best unimodal systems. For further improvement, our future work will project to use other biometric modalities

(Face and Iris) as well as the use of other fusion level like feature and decision levels. Also we will focus on the performance evaluation in both phases (verification and identification) by using a large size database.

REFERENCES

- A. Noore, R. S. and Vatsa, M. (2007). Robust memory-efficient data level information fusion of multi-modal biometric images. In *Information Fusion*. Vol. 8, No. 4, pp. 337-346.
- Angel Serrano, Isaac Martyn de Diego, C. C. E. C. (2010). Recent advances in face biometrics with gabor wavelets: A review. In *Pattern Recognition Letters*. Vol 31, pp. 372-381.
- Anil Jain, Karthik Nandakumar, A. R. (2005). Score normalization in multimodal biometric systems. In *Pattern Recognition*. Vol. 38, pp. 2270-2285.
- Cui, J.-R. (2012). Multispectral palmprint recognition using image based linear discriminant analysis. In *International Journal of Biometrics*. Vol. 4, No. 2, pp. 106-115.
- D. Zhang, V. Kanhangad, N. L. and Kumar, A. (2010). Robust palmprint verification using 2d and 3d features. In *Pattern Recognition*. Vol 43, No. 1, pp. 358-368.
- David Zhang, Zhenhua Guo, G. L. L. Z. and Zuo, W. (2010). An online system of multispectral palmprint verification. In *IEEE Transactions on Instrumentation and Measurement*. Vol. 59, No. 2, pp. 480-490.
- Harun Uguz, Ahmet Arslan, I. T. (2007). A biomedical system based on hidden markov model for diagnosis of the heart valve diseases. In *Pattern Recognition Letters*. Vol 28, pp. 395-404.
- Jinrong Cui, Y. X. (2011). Three dimensional palmprint recognition using linear discriminant analysis method. In *International Conference on Innovations in Bio-inspired Computing and Applications*. pp.107-111.
- PolyU. The hong kong polytechnic university multispectral palmprint database. www.comp.polyu.edu.hk/biometrics/MultispectralPalmprint/MSP.htm.
- Singh, A. P. and Mishra, A. (2011). Image de-noising using contourlets (a comparative study with wavelets). In *Int. J. Advanced Networking and Applications*. Vol. 03, Issue 03, pp. 1210-1214.
- Xian-Qian Wu, Kuan-Quan Wang, D. Z. (2003). Palmprint recognition using fishers linear discriminant. In *International Conference on Machine Learning and Cybermedcs*.